MSDE

PAPER

View Article Online
View Journal | View Issue

Cite this: *Mol. Syst. Des. Eng.*, 2022, 7, 1529

Predicting mixing free energy using mutual ghosting

Shreya Shetty,[a] Puja Agarwala,[a] Enrique D. Gomez[abc] and Scott T. Milner *[a]

Received 9th June 2022,
Accepted 9th August 2022

DOI: 10.1039/d2me00109h

rsc.li/molecular-engineering

The excess free energy of mixing ΔG_{ex} governs the phase behavior of mixtures and controls material properties. It is challenging, however, to measure ΔG_{ex} in simulations. Previously, we developed a method that combines molecular dynamics (MD) simulations with thermodynamic integration along the path of transformation of chains to predict the Flory Huggins interaction parameter χ for polymer mixtures and block copolymers. However, this method is best applied when the constituent molecules of the blends are structurally related. To overcome this limitation, we have developed a new method to predict ΔG_{ex} for mixtures. We perform simulations to induce phase separation within a mixture by gradually weakening the interaction between different species. To compute ΔG_{ex} we measure the thermodynamic work required to modify the interactions and the interfacial energy between the separated phases. We validate our method by applying it first to equimolar mixtures of labeled and unlabeled Lennard-Jones (LJ) beads, and labeled and unlabeled benzene, which results in good agreement with ideal solution theory. Then we compute the excess free energy of mixing for equimolar mixtures of benzene and pyridine, using both united-atom (UA) and all-atom (AA) potentials. Our results using UA potentials predict a value for ΔG_{ex} about four times the experimental value, whereas using AA potentials gives results consistent with experiment, highlighting the need for good potentials to faithfully represent mixture behavior.

Design, System, Application

Interactions between fluid species determine miscibility, phase behavior, and self-assembly. Computing interaction parameters ("chi parameters") from analytical theory is an insuperable task for all but the simplest idealized architectures. Molecular simulations would appear to be ideally suited for this task, as molecular shapes and interactions can be faithfully represented with properly designed simulation potentials. However, mixing free energies have entropic as well as enthalpic contributions, and so cannot be determined by simple time averages, but require special techniques, often involving thermodynamic integration. But not all thermodynamic integration pathways are equally suitable for measuring subtle intermolecular interactions on the scale of fractions of kT per molecule. In this work, we introduce a new, general approach to computing mixing free energies, for arbitrary molecular architectures. We demonstrate it first for model ideal solutions, then test it on a well-characterized miscible blend: benzene/pyridine. Our results demonstrate the utility and promise of the method—as well as the requirement that the simulation force fields faithfully represent the molecular mixture under study. We anticipate this method can be employed to study polymer blends, where determining chi from simulations for real polymer architectures remains a grand challenge.

1 Introduction

Most practical materials consist of more than one component, as mixtures offer unique properties that are not accessible using pure substances. In particular, polymer mixtures and block copolymers have made an impact in a variety of applications, including microelectronics, photovoltaics, membranes, biomimetic materials, and others.[1–6] The performance of these materials is strongly dependent on the structure and morphology of the blend.[7] A key challenge is thus to describe and predict the phase behavior of such mixtures.

The key factor governing the phase behavior of mixtures is the free energy of mixing ΔG_{mix}. For a two-component mixture,

$$\Delta G_{mix} = G_{12} - X_1 G_1 - X_2 G_2 \quad (1)$$

Here X_i and G_i are the mole fractions and free energy of species i, and G_{12} is the free energy of mixture.

As written in eqn (1), the mixing free energy ΔG_{mix} contains both the ideal and excess contributions. For mixtures reasonably described as regular solutions (*i.e.*, the constituent molecules are roughly the same size and shape), the excess mixing free energy ΔG_{ex} can be sensibly defined from

[a] *Department of Chemical Engineering, The Pennsylvania State University, University Park, PA, 16802, USA. E-mail: stm9@psu.edu*
[b] *Department of Materials Science and Engineering, The Pennsylvania State University, University Park, PA, 16802, USA*
[c] *Materials Research Institute, The Pennsylvania State University, University Park, PA, 16802, USA*

$$\Delta G_{mix} = \Delta G_{ex} + \Delta G_{ideal}$$
$$\Delta G_{ideal} = -kT(X_1 \log X_1 + X_2 \log X_2) \quad (2)$$

Here ΔG_{ideal} corresponds to the limiting case of an ideal solution, in which the two components are physically identical except for some innocuous label (the closest physical example being a mixture of hydrogenated and deuterated solvents).

In turn, the excess mixing free energy is often used to define an interaction parameter χ, which for regular solutions is typically written

$$\beta \Delta G_{ex} = X_1 X_2 \chi \quad (3)$$

(So defined, χ is not constant in general, but may depend on temperature, pressure, and composition).

Predicting ΔG_{ex} for mixtures is a challenging task. Many experiments, calculations, and simulations have been performed to determine ΔG_{ex} or equivalently χ, particularly for polymer blends.[8–16]

At first sight, atomistic molecular dynamics (MD) simulations appear well suited to the task of computing mixing free energies for chemically realistic solutions, since the energetic and entropic contributions to mixing depend on details of molecular shape and interactions, which simulations aspire to accurately describe.

However, MD simulations only give easy access to quantities that can be computed from particle positions and momenta; the energy is such a quantity, but the entropy and free energy are not. Thus special methods are always required to extract free energies from simulations.

In previous approach, we developed a "morphing" method to determine excess mixing free energies (and thus χ) for polymer mixtures.[17–20] In this approach, we perform molecular dynamic (MD) simulations for a sequence of systems, along which sequence one species of molecule is progressively transformed or "morphed" into another. We compute the work to transform the species by thermodynamic integration, and determine mixing free energies by comparing the work to morph molecules in a blend and in the pure state.

We have applied this method to bead-spring polymer chains, we have studied the effect of various factors like chain stiffness, interaction mismatch, and chain architecture on χ. For chain of different stiffness, Kozuch *et al.* found a positive entropic contribution to χ, in agreement with the field theory predictions of Fredrickson *et al.*[12,17] Zhang *et al.* studied the effect of Lennard Jones (LJ) interaction mismatch on χ, and validated their results by comparing the interfacial profile for immiscible blends predicted by self-consistent field theory (SCFT) with MD simulation results.[18] Shetty *et al.* studied the effect of chain architecture on χ, investigating blends with a more weakly-interacting bead located at different positions on polypropylene-like bead-spring chains.[19]

We have also extended the morphing method to chemically realistic polymers, predicting χ for four real polymer blends.[20] To carry out "atomistic morphing", we perform MD simulations for a sequence of systems along which the forcefield parameters of the molecules are progressively transformed from one species to another. This is evidently more complicated for real polymers than for bead-spring chains. We are obliged to adjust LJ parameters and partial charges, change bonded interactions as double bonds morph into single bonds, and sometimes progressively delete atoms altogether.

In this work, we explored a sequence of examples for which the experimental χ value progressively decreased. We thereby determined the practical limits to the atomistic morphing method, which reflect both statistical error (which becomes more demanding for small χ) and systematic error in the force fields. In brief, the method holds promise for χ values down to of order 10^{-2}. However, atomistic morphing has another practical limitation: different species in the mixture must be structurally related. For mixtures involving species that are only distantly related structurally, atomistic morphing requires increasingly complicated schemes in which many moieties are morphed, added, or removed to transform one polymer species into another. This quickly becomes impractical for all but the most structurally similar pairs of polymers.

To overcome the limitation of structural similarity, in this study we present a new method called "mutual ghosting" to predict the excess free energy of mixing ΔG_{ex}. Mutual ghosting works by progressively weakening the interactions between two species in a miscible blend, until they undergo phase separation (as the mutual interactions weaken, the two species become "ghosts" to each other). We can compute the work to achieve phase separation by thermodynamic integration.

However, the state induced by weakened interactions is not complete phase separation, in two respects: 1) an interface between the separated phases is present, and 2) a dilute amount of species A may be present in the B-rich phase, and *vice versa*. To determine the work to completely separate the two species, we must measure the interfacial tension of the A–B interface, and compute the work to "sweep" the dilute stragglers into their own phase.

The mixing free energy ΔG_{mix} that we seek is then the negative of the total work ΔG_{demix} to completely demix the system into its pure components, given by

$$\Delta G_{demix} = \Delta G_{weak} - \Delta G_{int} + \Delta G_{sweep} \quad (4)$$

Here ΔG_{weak} is the thermodynamic work to weaken the A–B interactions; $\Delta G_{int} = 2A\gamma$ is the A–B interfacial free energy (two interfaces in a periodic system of cross-sectional area A), and ΔG_{sweep} is the work to transfer the stragglers (see Appendix for details).

The mutual ghosting method gives the full mixing free energy ΔG_{mix}; to obtain the excess free energy of mixing ΔG_{ex}, we must subtract the ideal contribution. This imposes a limitation on the sensitivity of the method; to measure weak deviations from ideal mixing, we must measure ΔG_{mix} quite accurately.

To test our new method, we first apply it to ideal mixtures, for which the excess free energy of mixing ΔG_{ex} should vanish. The simplest such system is an equimolar mixture of Lennard Jones (LJ) beads, differing only in their labels A and B. For a simple chemically specific ideal mixture, we likewise apply mutual ghosting to an equimolar mixture of labeled and unlabeled benzene.

We then apply our method to an equimolar benzene–pyridine mixture. Benzene and pyridine have very similar molecular shapes, but rather different interactions because of the substantial dipole on pyridine (about 2.2 Debye); thus such mixtures serve as a good example of a regular solution, for which the mixing free energy can be written as in eqn (2). Also, vapor–liquid equilibrium (VLE) data is available for benzene–pyridine solutions; VLE data can be used to infer the mixing free energy, for comparison of our mutual ghosting results to experiment.

As with any simulation method, our results depend on the force field we use to represent the molecules being simulated. For benzene and pyridine, we investigate both united atom (TraPPE UA) and all-atom (OPLS-AA) potentials. Both have been well tested for the respective pure fluids, but neither have been specifically tested or tuned for benzene–pyridine mixtures.

To distinguish between shortcomings of the potentials in describing real molecules and difficulties with the mutual ghosting method, it is useful to compare to results for χ obtained with other simulation methods using the same potentials. Because they are structurally so similar, χ for benzene and pyridine described by both UA and AA potentials can readily be obtained using atomistic morphings.

2 Methods

The mutual ghosting method consists of a sequence of MD simulations in which attractive interactions between two species in a mixture are progressively weakened, which causes the species to demix. The work to demix ΔG_{demix} is computed by thermodynamic integration; the interfacial tension γ between the resulting phases is measured by standard techniques. Finally, the work ΔG_{sweep} to transfer species A molecules from the B-rich phase to the A-rich phase and *vice versa* is computed from the concentrations of these "straggler" molecules. The mixing free energy ΔG_{mix} is then given in terms of these results by eqn (4).

To illustrate mutual ghosting in detail, we apply it to the simplest ideal mixture, an equimolar mixture of pointlike particles interacting with identical LJ interactions, differing only in their labels. For an ideal mixture, we expect ΔG_{mix} to be given by the ideal-mixing result, which serves as a first test of our method.

2.1 Ideal solution of LJ beads

Our first model ideal solution consists of a liquid of LJ beads with diameter σ = 0.2 nm, and interaction strength ε equal to kT at the simulation temperature of 300 K (*i.e.*, ε = 2.49 kJ mol^{-1}), at a pressure of 1 bar.

To build the equilibrated solution, we first randomly insert 5000 LJ beads into a cubic simulation box of linear dimension 6 nm. We randomly label the beads as species A and B. We then minimize the system energy, followed by simulation at fixed NPT for 5 ns.

All simulations were performed using GROMACS.[21] These simulations run at 250 ns per day on 8 cores with 1 GPU, with a timestep of 1 fs. The particles diffuse at a rate of 6.9 nm^2 ns^{-1}, so that 5 ns is more than adequate to equilibrate the species concentrations. Fig. 1(a) displays a snapshot of the resulting solution, in which A beads are shown as red and B as blue.

We then perform a series of simulations in which the LJ interaction strength between red and blue beads is systematically decreased, while blue–blue and red–red interactions remain the same. As the interactions between blue and red beads weaken, beads of the same species increasingly cluster together, ultimately separating into immiscible phases (see Fig. 1(b)).

The weakening of the LJ interactions between red and blue beads is controlled by a parameter λ:

$$\mathrm{LJ}(r,\lambda) = (1-\lambda)\left(\frac{C^{(12)}}{r^{12}} - \frac{C^{(6)}}{r^{6}}\right) \tag{5}$$

Here $C^{(12)} = 4\varepsilon\sigma^{12}$ and $C^{(6)} = 4\varepsilon\sigma^{6}$, where σ and ε are the LJ diameter and interaction energy.

To modify nonbonded interactions between two species A and B while leaving A–A and B–B interactions undisturbed, the only practical way is to use tabulated interactions, with separate tables for A–B and all other interactions. This approach works for molecules of arbitrary complexity, and handles Coulomb as well as LJ interactions. In GROMACS, this can be done with .mdp options
coulombtype = User
vdwtype = User
energygrps = A B
with index groups A and B defining species A and B.

The A–B table table_A_B.xvg is computed from the standard table table6-12.xvg with all entries multiplied by 1 − λ. More precisely, we used a "soft cutoff" scheme in which the potential singularity at r = 0 is softened as λ becomes small.[22] The soft-cutoff potential we used takes the form

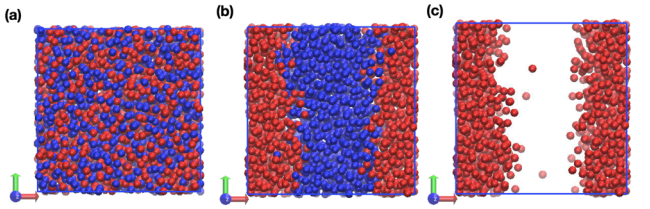

Fig. 1 Snapshots of the (a) equilibrated LJ beads melt, (b) after phase separation and (c) with only red beads.

$$V_{sc}(r) = (1-\lambda)V(r_{sc})$$
$$r_{sc} = (\alpha\sigma_{sc}{}^6\lambda + r^6)^{1/6} \quad (6)$$

with $\alpha = 0.5$ and $\sigma_{sc} = 0.2$ nm. This potential avoids problems that occur when nearly-vanished particles have insufficient repulsive interactions to prevent other particles from approaching their weak but still singular potential at $r = 0$.

The work dW to weaken the interactions by $\partial\lambda$ at λ is given by $dW = \partial G/\partial\lambda$, with the latter derivative given by

$$\left(\frac{\partial G}{\partial \lambda}\right) = \left\langle \frac{\partial H}{\partial \lambda}\right\rangle_\lambda \approx \frac{\langle \Delta H\rangle_\lambda}{\Delta\lambda} \quad (7)$$

in which H_λ is the system Hamiltonian at a given value of λ. Physically, eqn (7) says the generalized thermodynamic force $\partial G/\partial\lambda$ acting through a small displacement $\Delta\lambda$ equals the average change in system energy $\langle\Delta H\rangle$, which is the work done.

We emphasize that the first equality in eqn (7) is thermodynamically exact, derivable from the appropriate partition function. Indeed, this same general relation is used for atomistic morphing, in which λ controls the morphed atomistic parameters. For the Gibbs ensemble, the thermodynamic work of eqn (7) includes the effects of volume change on mixing (to see this, note that only the Hamiltonian depends on the morphing parameter λ, while the system volume is a property of the microstate), which in any case are very small for most regular solutions.

The sequence of λ values is chosen to reasonably represent the integrand eqn (7). The last frame of the simulation at a given λ is used as the initial configuration for the next λ value, which is a sensible procedure if the λ values are closely spaced, and the ensembles at neighboring λ values overlap significantly.

We evaluate the derivative $\langle\partial H/\partial\lambda\rangle$ using a finite difference between adjacent λ values (last line in eqn (7)). In detail, we compute ΔE_λ by rerunning the simulation trajectory at a given λ with the interaction tables corresponding to neighboring λ values, and taking the difference of the average energy in the original and rerun.

Fig. 2(a) displays results for the integrand $\partial G/\partial\lambda$ *versus* λ for our LJ beads ideal solution. The points in the graph indicate the λ values taken, which are chosen to give good representation of the integrand. To ensure good averaging of the integrand, each λ value corresponds to a simulation run of 20 ns.

To compute the free energy ΔG_{weak} to weaken the interactions, we integrate the generalized thermodynamic force $\partial G/\partial\lambda$ with respect to λ; Fig. 2(b) presents the integral *versus* λ. Evidently, as λ progressively increases and we continue to weaken the A–B interaction, the work to demix continues to increase. Because A and B have largely separated beyond about $\lambda = 0.3$, this reflects the increase in interfacial tension as the A–B interactions weaken.

To completely demix the system, we must remove the interface between the two phases. To this end, we measure the interfacial tension γ in terms of the pressure anisotropy in the usual way, as

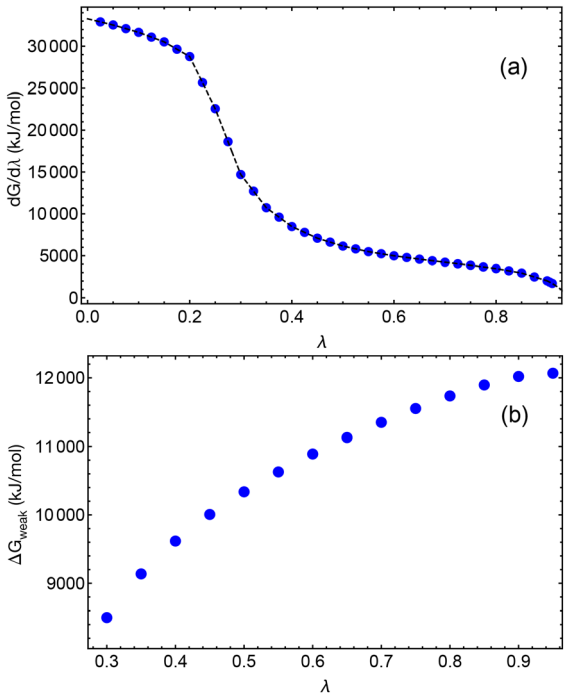

Fig. 2 (a) Free energy integrand $dG/d\lambda$ *versus* λ and (b) free energy to weaken interactions ΔG_{weak} *versus* λ for bead–bead separation.

$$2\gamma/L = P_z - (1/2)(P_x + P_y) \quad (8)$$

for interfaces normal to the z axis in a cubic cell of linear dimension L. The total interfacial free energy ΔG_γ is then $2\gamma A$ (there are two interfaces of area $A = L^2$ in the periodic system), which increases with λ as shown in Fig. 3.

Comparing Fig. 3 and 2(b), we see that the increasing work to effect the phase separation at larger values of λ is nearly identical to the increasing free energy of the A–B interface. This suggests that when the work to achieve phase separation is computed *via* eqn (4), the result will be nearly constant with λ.

Even after the A–B interfacial tension is accounted for, the phase separation induced by weakening the A–B interactions is not complete; for a system of small molecules, a few "stragglers" of species A may be present in the B-rich phase,

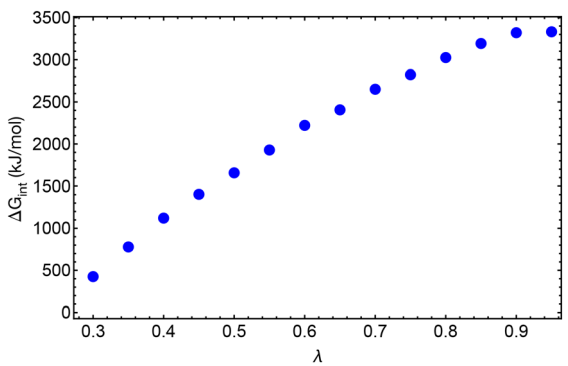

Fig. 3 Interfacial free energy ΔG_{int} *versus* λ for LJ beads mixing.

or *vice versa*. This is the case for our LJ bead simulations, as shown in Fig. 4(a). We count the stragglers by integrating the number density in each phase, and calculate the work ΔG_{sweep} to transfer or "sweep" the stragglers to their own phase, which turns out to be kT per particle (see Appendix for details). Fig. 4(b) shows how ΔG_{sweep} depends on λ; as λ increases, the phase separation is more complete, and fewer stragglers remain to be swept into the proper phase.

We determine the free energy of mixing ΔG_{mix}, or rather its negative, the free energy of de-mixing ΔG_{demix}, from the measured values using eqn (4). We obtain ΔG_{ex} from ΔG_{mix} by subtracting the ideal part of the mixing free energy, using eqn (2).

Putting together our results for the work ΔG_{weak} to weaken the A–B interactions, the interfacial free energy ΔG_{int}, and the work ΔG_{sweep} to sweep the stragglers into the appropriate phase, we obtain the work to completely demix the system ΔG_{demix}, which is the negative of ΔG_{mix} (see Fig. 5). As evident in the figure, the demixing free energy for this ideal solution is independent of λ (above $\lambda \approx 0.3$, at which phase separation first occurs), and consistent with the ideal-mixing result $\Delta G_{ideal} = kT \log 2$.

The individual contributions to ΔG_{demix} each vary with λ—the work ΔG_{weak} to weaken the A–B interaction increases (Fig. 2), the interfacial free energy ΔG_{int} likewise increases in nearly the same way (Fig. 3), and the small work ΔG_{sweep} to sweep the stragglers out decreases (Fig. 4)—but the sum is quite constant. We can thus improve our value for ΔG_{demix} by averaging the independent values, and estimate our statistical error from the variance. From simulations, ΔG_{demix} = 1.738 ± 0.009 kJ mol^{-1} for LJ beads separation from itself, consistent with the expected $kT \log 2$ = 1.729 kJ mol^{-1} within the small statistical error.

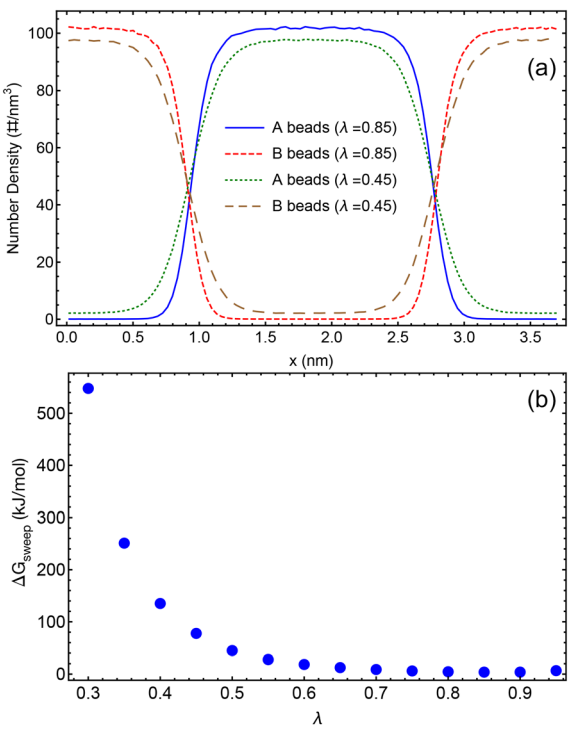

Fig. 4 (a) Number density of beads *versus* box co-ordinate at two λ values and (b) work to sweep ΔG_{sweep} *versus* λ.

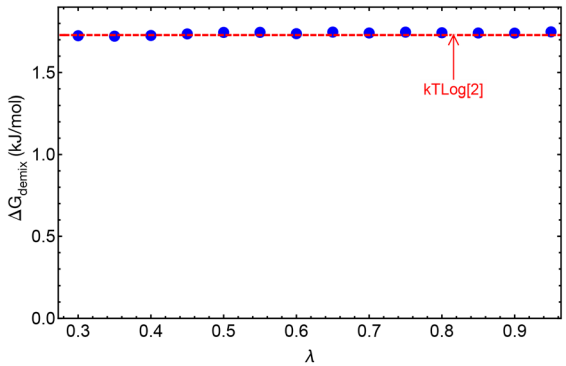

Fig. 5 Demixing free energy ΔG_{demix} per bead *versus* λ for ideal solution of LJ beads.

2.2 Benzene and pyridine mixtures

For molecular mixtures, we consider an ideal solution of equimolar labeled and unlabeled benzene, followed by an equimolar mixture of benzene and pyridine, as a good representation of a regular solution.

To prepare the equilibrated initial state of a benzene–benzene ideal solution, we begin by randomly inserting 2500 benzene molecules into a cubic simulation box of linear dimension 10 nm. To equilibrate, we 1) minimize the energy, 2) resize the system to the experimental density during a 1 ns simulation, and 3) equilibrate for 1 ns under NPT conditions at 300 K at 1 bar pressure. For the benzene ideal solution, we use OPLS-AA (Optimized Potentials for Liquid Simulations-All Atom) potentials.[23]

We prepare equimolar benzene–pyridine solutions in the same way, using 1250 benzene and 1250 pyridine molecules in a cubic 10 nm simulation box. We perform benzene–pyridine mutual ghosting simulations using the united-atom TraPPE (Transferable Potentials for Phase Equilibria Force Field) potential, as well as the all-atom OPLS-AA potential, to see how the two potentials compare in their predictions.[24,25]

Our MD simulations for benzene and pyridine employ a timestep of 1 fs, and run at 25 ns per day on 16 cores with 1 GPU. Each λ value in the sequence of mutual ghosting simulations is run for 50 ns. Benzene diffuses in our simulations at a rate of about 1.7 nm^2 ns^{-1} (in good agreement with the experimental value of 2.2 nm^2 ns^{-1}), so runs of this length are more than sufficient to equilibrate concentration fluctuations across the system.

Finally, we perform atomistic morphing simulations[20] to compute the mixing free energy for benzene–pyridine solutions by a completely independent route, to compare with our mutual ghosting results using the same TraPPE and OPLS-AA force fields.

To summarize the atomistic morphing method, starting with a pure benzene liquid, we perform two series of

simulations, in which we transform either all or half of the benzene molecules to pyridine, to obtain either pure pyridine or an equimolar benzene–pyridine solution. By thermodynamic integration with respect to the morphing parameter λ, we compute the work to effect each transformation, and thereby calculate ΔG_{pyr} and $\Delta G_{benz-pyr}$, with pure benzene as the reference state. The excess mixing free energy ΔG_{ex} is given by

$$\Delta G_{ex} = \Delta G_{benz-pyr} - (1/2)\Delta G_{pyr} \quad (9)$$

Note that atomistic morphing although more cumbersome and less general than mutual ghosting because it requires structural similarity between species, has the advantage that it gives the excess mixing free energy directly, with no need to subtract the ideal mixing contribution.

3 Results

3.1 Benzene ideal solutions

Following the same procedures described in section 2.1 and illustrated for the ideal solution of labeled and unlabeled LJ beads, we perform mutual ghosting simulations for ideal equimolar solutions of labeled and unlabeled benzene. Fig. 6(a) displays results for the free energy ΔG_{weak} to weaken the interactions between labeled and unlabeled molecules, and Fig. 6(b) displays the interfacial free energy ΔG_{int}, both as a function of λ.

In contrast to our results for ideal solutions of LJ beads, for benzene–benzene ideal solutions we find no "straggler" molecules in the wrong phase (presumably because the interactions per molecule are larger compared to kT for benzene than for our LJ beads). Hence for these molecular solutions, we do not need to correct for the work to transfer stragglers to the appropriate phase.

Fig. 7 shows the demixing free energy ΔG_{demix} per molecule *versus* λ for ideal solutions of benzene in benzene. As for the LJ bead ideal solution results, the demixing free energy is independent of λ once phase separation has occurred, with the increase in interfacial free energy ΔG_{int} compensating precisely for the increase in the work ΔG_{weak} to weaken the interactions. Averaging the data points in Fig. 7, we find $\Delta G_{demix} = 1.713 \pm 0.005$ kJ mol^{-1}, reasonably consistent with the ideal solution result of $\Delta G_{ideal} = kT \log 2 = 1.729$ kJ mol^{-1}.

3.2 Benzene–pyridine solutions

We perform mutual ghosting simulations for equimolar benzene–pyridine solutions using united-atom TraPPE as well as all-atom OPLS-AA potentials. Fig. 8(a) and (b) presents our results for the work to weaken the interactions ΔG_{weak} and the free energy ΔG_{int} of the resulting interface, for both potentials (as for benzene ideal solutions, we observe no straggler molecules in the wrong phase, so no correction is required to account for sweeping stragglers into the correct phase).

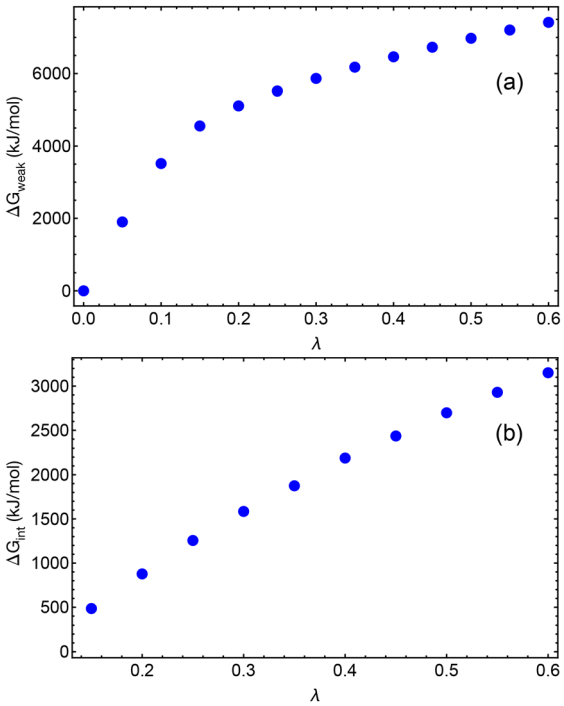

Fig. 6 (a) Free energy to weaken interactions ΔG_{weak} as a function of λ and (b) interfacial free energy ΔG_{int} *versus* λ for benzene–benzene mixture.

For both potentials, we again find that as we weaken the interactions between benzene and pyridine, the work ΔG_{weak} increases in the same way as the interfacial free energy ΔG_{int}. As a consequence, the demixing free energy predicted using either potential is constant over the range of λ for which the mixture has separated (see Fig. 9).

However, our results using TraPPE UA and OPLS-AA potentials differ substantially from each other: using TraPPE potentials, we find ΔG_{ex} equal to 0.49 ± 0.01 kJ mol^{-1}, while for OPLS-AA potentials we obtain a much smaller value of 0.17 ± 0.01 kJ mol^{-1}. The latter result is much closer to the experimental value of 0.125 kJ mol^{-1}, obtained from fitting vapor–liquid equilibrium (VLE) data for benzene–pyridine solutions to regular solution theory.[26]

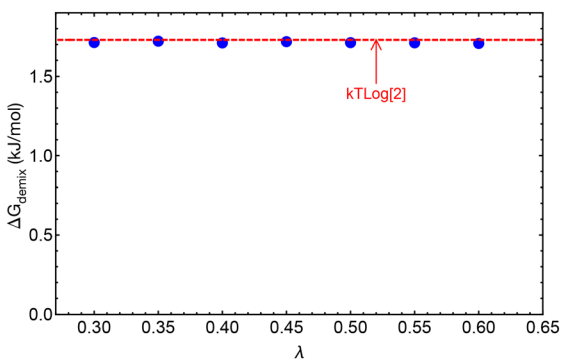

Fig. 7 Demix free energy ΔG_{demix} per molecule *versus* λ for benzene–benzene mixture.

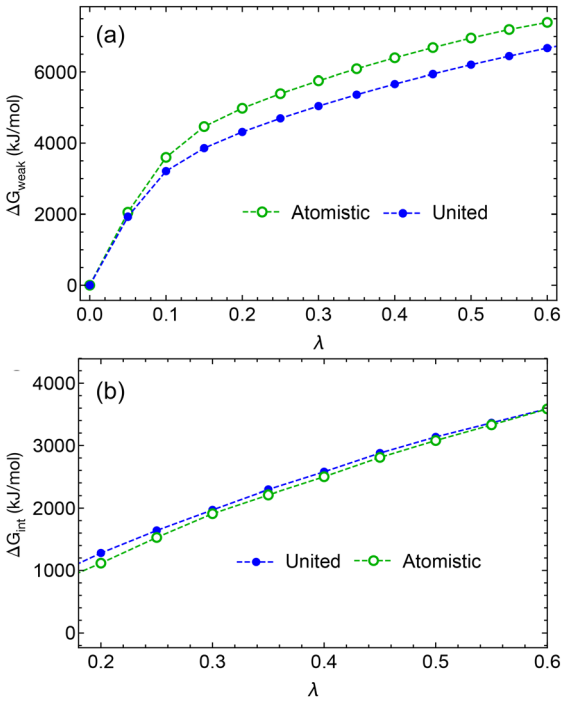

Fig. 8 (a) Free energy to weaken interactions ΔG_{weak} as a function of λ and (b) interfacial free energy ΔG_{int} *versus* λ for benzene–pyridine, using TraPPE UA (blue, filled circles) and OPLS-AA (green, open circles) potentials.

So is the discrepancy between mutual ghosting results using TraPPE and OPLS potentials (and between both these results and experiment) evidence of a shortcoming in the method, or in the potentials? To shed light on this question, we performed atomistic morphing simulations for an equimolar benzene–pyridine solution of 2500 molecules, using the same potentials.

Fig. 10 displays the results of atomistic morphing simulations for the free energy integrand $\partial G_{ex}/\partial\lambda$ for TraPPE UA and OPLS-AA potentials. As evident from the figure, the area under the curve is larger for the TraPPE results. Performing the integral to obtain ΔG_{ex}, we find ΔG_{ex} = 0.375 ± 0.005 kJ mol^{-1} for TraPPE potentials, *versus* 0.165 kJ mol^{-1} for OPLS-AA

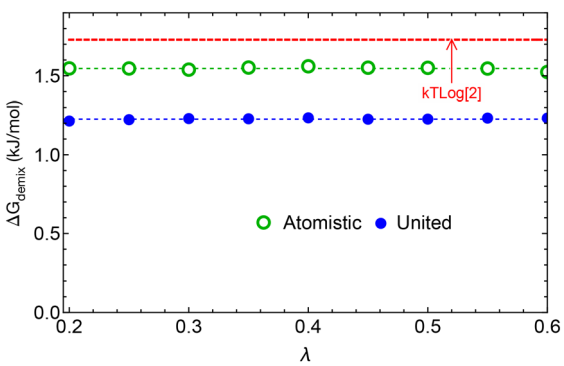

Fig. 9 Demix free energy ΔG_{demix} per molecule *versus* λ for benzene–pyridine mixture, using TraPPE UA (blue, filled circles) and OPLS-AA (green, open circles) potentials.

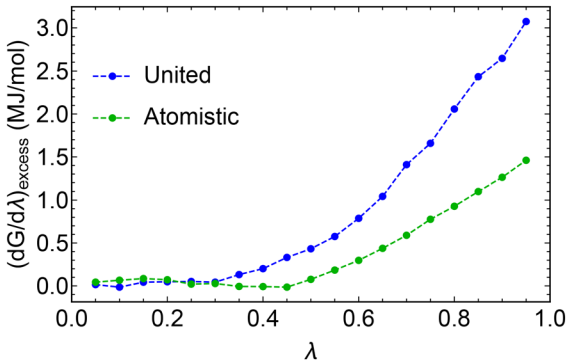

Fig. 10 Excess free energy integrand $\partial G_{ex}/\partial\lambda$ *versus* λ for benzene–pyridine mixture from "atomistic morphing" simulations, using TraPPE UA (blue) and OPLS-AA (green) potentials.

potentials. These atomistic morphing results, using a completely different approach, are consistent with our mutual ghosting results, in the following respects: a) the TraPPE-derived value is much higher than the OPLS-AA value, b) the OPLS-AA values from atomistic morphing and mutual ghosting are in close agreement, and c) the OPLS-AA values are in much better although not perfect agreement with experiment.

Table 1 summarizes our results obtained using both potentials, with both methods, reported both as excess mixing free energies, and as χ parameters on a per molecule basis, obtained from eqn (3). Error bars for simulation ΔG_{ex} results (both UA and AA) are 0.01.

4 Conclusion

We present a new "mutual ghosting" simulation method to determine the free energy of mixing ΔG_{mix} for miscible solutions. The new method works by artificially weakening the interactions between species A and B to induce phase separation, then measures the interfacial tension between the immiscible phases. The work ΔG_{demix} to demix the two species (which equals $-\Delta G_{mix}$) is the sum of the work ΔG_{weak} to weaken the interactions, minus the interfacial free energy ΔG_{int}. ΔG_{demix} can be computed by thermodynamic integration along the path of weakening interactions. Sometimes, a dilute admixture of "straggler" molecules of species A remains in the B-rich phase, and *vice versa*; in such cases, we add to ΔG_{demix} the thermodynamic work ΔG_{sweep} to sweep these stragglers to the appropriate phase, to complete the separation of A and B.

Table 1 Excess mixing free energy results for benzene–pyridine solutions, computed using TraPPE and OPLS-AA potentials, by mutual ghosting (top values) and atomistic morphing (bottom values)

Source	ΔG_{ex} (kJ mol^{-1})	χ
TraPPE UA	0.49	0.79
	0.38	0.61
OPLS-AA	0.17	0.27
	0.17	0.27
Experiment	0.125	0.2

Mutual ghosting overcomes an important limitation of our previously developed "atomistic morphing" method,[20] which determines the excess free energy of mixing ΔG_{ex} from simulations by computing the work to progressively transform one species into another, but in practice requires the two species to be closely related structurally. In contrast, mutual ghosting can applied to completely dissimilar species. However, atomistic morphing computes ΔG_{ex} directly, without subtracting the ideal mixing free energy ΔG_{ideal} from ΔG_{mix}, as must be done for mutual ghosting. For nearly-ideal mixtures, this imposes stringent requirements on the statistical error of mutual ghosting simulations.

We test our new method first by applying it to ideal solutions, first a mixture of labeled and unlabeled Lennard-Jones particles, then a mixture of labeled and unlabeled benzene. In both cases, we compute $\Delta G_{mix} = \Delta G_{ideal}$ to very good accuracy. For simplicity, in the present work we consider only equimolar mixtures; however, like the atomistic morphing method, the new mutual ghosting method can be applied equally well to non-equimolar mixtures.

Then, we apply mutual ghosting to equimolar benzene–pyridine solutions, which are convenient to study for several reasons: 1) because benzene and pyridine have similar size and shape, they are reasonably described as regular solutions; 2) because they are structurally similar, we can use atomistic morphing as well as mutual ghosting to determine ΔG_{ex} for the same force fields; and 3) experimental results for ΔG_{ex} can be inferred from published vapor–liquid equilibrium data.

As with any chemically specific simulation, our results rely on the fidelity of the force fields we use to model the system. In this work, we simulate benzene and pyridine using two different force fields, the TraPPE UA (united atom) and the OPLS-AA (all atom) force fields. Both are commonly used, both have been tested against pure fluid properties, and neither has been specifically tuned to represent benzene–pyridine mixtures.

We find that mutual ghosting simulations using TraPPE UA potentials predict ΔG_{ex} four times larger than experiment, while OPLS-AA potentials give values about 30 percent larger than experiment. Simulation results using atomistic morphing are reasonably consistent with mutual ghosting values, particularly for OPLS-AA potentials. This finding highlights the fact that simulation predictions for mixing free energies are only reliable if the underlying force fields reasonably represent the interacting species, and that validation of potentials for pure-fluid properties may not ensure good results for mixtures.

5 Appendix: sweeping up the stragglers

Consider a two component, phase separated system consisting of species A and B, with a dilute amount of B in A-rich phase and *vice versa*. For a system in equilibrium, the chemical potential μ_B of B molecules is same in both the phases ($\Delta\mu = 0$). As a result, the thermodynamic work $\Delta\mu$ to transfer a single B molecule from the A-rich phase to B-rich phase is initially zero.

However, as we continue to transfer B molecules, the concentration of B in the A phase drops, and the translational entropy of the remaining B molecules in the A-phase increases, given by eqn (10):

$$\Delta S(c) = -k\log(c/c_0) \tag{10}$$

Here c_0 is the equilibrium concentration of B in the A-rich phase, and c its reduced value after some transfers have taken place.

Hence, the work to transfer a B molecule to the B-rich phase as a function of its concentration in the A-rich phase is

$$\Delta\mu(c) = \Delta E - T\Delta S = -kT\log(c/c_0) \tag{11}$$

(We assume here that B molecules are dilute enough in the A-rich phase that they may be regarded as an ideal solute, and interactions between B molecules in the A-rich phase neglected). The same arguments hold true for dilute A molecules in B-rich phase.

We integrate to find the work to transfer all the B molecules to B-rich phase (assuming the dilute concentration of A in the B-rich phase is largely unaffected, since very few B molecules are transferred). The work per unit volume is then

$$W/V = \int_0^{c_0} \mathrm{d}c\Delta\mu(c) = kTc_0 \tag{12}$$

Correspondingly, the work per particle transferred is simply kT.

Conflicts of interest

There are no conflicts to declare.

Acknowledgements

Financial support from the National Science Foundation under awards DMREF-1629006, DMREF-1921854, and DMR-1905632 are acknowledged.

Notes and references

1 M. T. Shaw, *Polym. Eng. Sci.*, 1982, **22**, 115–123.
2 C. M. Bates and F. S. Bates, *Macromolecules*, 2017, **50**, 3–22.
3 L. M. Robeson, *Polym. Eng. Sci.*, 1984, **24**, 587–597.
4 I. W. Hamley, *Nanotechnology*, 2003, **14**, R39–R54.
5 M. Sommer, S. Huettner and M. Thelakkat, *J. Mater. Chem.*, 2010, **20**, 10788–10797.
6 S. Aid, A. Eddhahak, S. Khelladi, Z. Ortega, S. Chaabani and A. Tcharkhtchi, *Polym. Test.*, 2019, **73**, 222–231.
7 C. W. Macosko, *Macromol. Symp.*, 2000, **149**, 171–184.
8 T. Nishi and T. T. Wang, *Macromolecules*, 1975, **8**, 909–915.
9 C. Kim and D. Paul, *Polymer*, 1992, **33**, 1630–1639.
10 O. Olabisi, *Macromolecules*, 1975, **8**, 316–322.
11 L. Leibler, *Macromolecules*, 1980, **13**, 1602–1617.

12 G. H. Fredrickson, A. J. Liu and F. S. Bates, *Macromolecules*, 1994, 2503–2511.
13 E. Helfand and Y. Tagami, *J. Polym. Sci., Part B: Polym. Lett.*, 1971, **9**, 741–746.
14 A. Chremos, A. Nikoubashman and A. Z. Panagiotopoulos, *J. Chem. Phys.*, 2014, **140**, 054909.
15 C. P. Callaway, K. Hendrickson, N. Bond, S. M. Lee, P. Sood and S. S. Jang, *ChemPhysChem*, 2018, **19**, 1655–1664.
16 Q. P. Chen, J. D. Chu, R. F. DeJaco, T. P. Lodge and J. I. Siepmann, *Macromolecules*, 2016, **49**, 3975–3985.
17 D. Kozuch, W. Zhang and S. Milner, *Polymer*, 2016, **8**, 241.
18 W. Zhang, E. D. Gomez and S. T. Milner, *Phys. Rev. Lett.*, 2017, **119**, 017801.
19 S. Shetty, M. M. Adams, E. D. Gomez and S. T. Milner, *Macromolecules*, 2020, **53**, 9386–9396.
20 S. Shetty, E. D. Gomez and S. T. Milner, *Macromolecules*, 2021, **54**, 10447–10455.
21 B. Hess, C. Kutzner, D. van der Spoel and E. Lindahl, *J. Chem. Theory Comput.*, 2008, **4**, 435–447.
22 T. C. Beutler, A. E. Mark, R. C. van Schaik, P. R. Greber and W. F. van Gusteren, *Chem. Phys. Lett.*, 1994, **222**, 529–539.
23 W. L. Jorgensen and D. L. Severance, *J. Am. Chem. Soc.*, 1990, **112**, 4768–4774.
24 C. D. Wick, J. M. Stubbs, N. Rai and J. I. Siepmann, *J. Phys. Chem. B*, 2005, **109**, 18974–18982.
25 C. D. Wick, M. G. Martin and J. I. Siepmann, *J. Phys. Chem. B*, 2000, **104**, 8008–8016.
26 P. Garrett, J. Pollock and K. Morcom, *J. Chem. Thermodyn.*, 1973, **5**, 569–575.